

On the sensitivity improvement of CMOS capacitive accelerometer

Chih-ming Sun^a, ChuanWei Wang^b, Weileun Fang^{a,b,*}

^a Institute of NanoEngineering and Microsystems, National Tsing Hua University, Hsinchu, Taiwan

^b Department of Power Mechanical Engineering, National Tsing Hua University, Hsinchu, Taiwan

Received 15 March 2007; received in revised form 5 October 2007; accepted 5 October 2007

Available online 17 October 2007

Abstract

This study presents an improved CMOS capacitive accelerometer design. In this design, the sensitivity has been increased by adding the number of sensing finger arrays. Moreover, the present accelerometer successfully employs the additional springs and post on CMOS chip for electrical routing of sensing fingers. In general, the present study enables the increasing of sensing capacitance by 80%, at the cost of the decreasing of proof mass by 20%. Thus, the net sensitivity of the accelerometer will still be increased by 1.44-fold without changing its die size. As to the accelerometers of the same fundamental frequency, the sensitivity of the present design can even be increased by 1.8-fold without changing its die size. The measurement results show that the sensitivity and the nonlinearity of a typical improved accelerometer are 3.95 mV/G, and 2.75%, respectively. As a comparison, the existing accelerometer of the same die size and fundamental frequency (i.e. stiffness to mass ratio) has the sensitivity and the nonlinearity of 2.10 mV/G, and 2.87%, respectively. The results demonstrate that the present design has successfully improved the sensitivity of the CMOS capacitance accelerometer by 1.88-fold.

© 2007 Elsevier B.V. All rights reserved.

Keyword: CMOS capacitive accelerometer

1. Introduction

The standard CMOS process has been extensively applied to fabricate MEMS devices. The major advantage of the CMOS process is the monolithic integration of the IC and MEMS components. Moreover, the stable foundry service is ready for CMOS process. The CMOS MEMS processes can be categorized as pre-CMOS [1], intermediate-CMOS [2], and post-CMOS processes [3], respectively. In general, the post-CMOS is the most popular approach since the changing of standard CMOS process is not required. The applications of standard CMOS process and special post-CMOS processes on MEMS have been reported [4,5]. Nevertheless, the process sequence, film materials and thickness, and layout rule have been strictly defined by the foundry-service CMOS process. Moreover, the thin film residual stresses resulted from the processes frequently lead to unwanted deformation to the suspended CMOS MEMS structures. Thus, the design of MEMS components remains significantly limited by this standard process.

The CMOS MEMS technology has already found various applications in the area of micro sensors, for instance, the accelerometer [4–7], the pressure sensor [8], the IR sensor [9], the gyroscope [10,11], the gas sensor [12], etc. Presently, various capacitance type linear accelerometers implemented using the standard CMOS process have been reported [4–7]. In addition to capacitance sensing, the piezoresistive [13], thermal [14], and optical [15] CMOS accelerometers have also been reported. Due to the integration of sensing circuit and MEMS transducer on the chip, CMOS MEMS accelerometers have advantages over hybrid solution of smaller die size, less noise and higher ability to integrate for semi-custom applications. In general, the sensitivity of the capacitive accelerometer can be improved by increasing the proof mass and the number of sensing fingers, and decreasing the spring stiffness. However, the die size and the yield during the post-CMOS process are also critical design considerations.

The goal of this study is to improve the sensitivity of the existing CMOS capacitance type linear accelerometer [4,5] without changing the die size. To this end, the present accelerometer design significantly increases the sensing capacitance by adding the number of sensing electrodes. Meanwhile, the proof mass will slightly decrease to ensure the die size remaining unchanged. In addition, the critical design of spring and

* Corresponding author. Tel.: +886 3 574 2923; fax: +886 3 572 2840.
E-mail address: fang@pme.nthu.edu.tw (W. Fang).

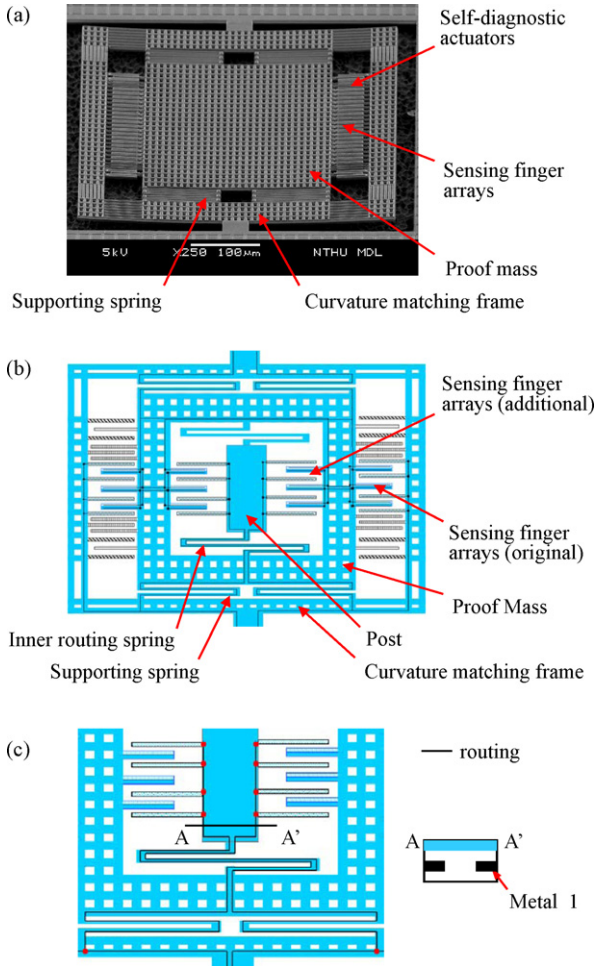


Fig. 1. (a) The existing accelerometer design with two sensing finger arrays, (b) the schematic illustration of the present accelerometer with additional sensing electrode arrays on a hollow proof mass, and (c) the inner springs act as the electrical routing for stationary electrodes on post.

anchor-post on CMOS chip are also introduced for electrical routing of sensing fingers. The accelerometer has been implemented using TSMC 2P4M process plus the post-release technique. The performance of present accelerometer has also been demonstrated by comparing with the existing design.

2. Design and analysis

Fig. 1a shows the existing CMOS capacitance accelerometer originated with Refs. [4,5]. This accelerometer consists of a proof mass, supporting springs, sensing electrodes, self-diagnostic actuators, and curvature matching frame. The proof

mass of the spring-mass system will be excited after subjecting to the acceleration. Thus, the motion of the proof mass will lead to the capacitance change of sensing electrodes, so as to determine the acceleration. This study reports the accelerometer design in Fig. 1b to further improve the sensitivity of the accelerometer in Fig. 1a.

The present accelerometer is based on the 2P4M TSMC 0.35 μm CMOS process to monolithically integrate the MEMS structure and the sensing circuits. In short, the present accelerometer design removes the center part of the proof mass, and replace with the sensing electrode arrays to increase its sensitivity. As shown in Fig. 1b, this design contains a hollow proof mass. A post, which located at the center of the hollow proof mass, is anchored to the substrate. There are additional stationary electrodes fixed to the post, and additional moving electrodes added to the inner edges of the proof mass. Thus, the motion of the proof mass will be detected by both the inner and outer sensing electrodes. The proof mass connects to the post as well as the substrate through inner springs. These inner springs act as the electrical routing for the stationary electrodes on post, as shown in Fig. 1c.

Fig. 2 shows the gain flow chart of the present design, which indicates gains respectively yielded from four different means. In Fig. 2, the parameter A_{cc} is the acceleration to be measured, ΔX is the displacement of the proof mass, ΔC is the net capacitance change for one sensing electrode pair (one stationary plus one moving electrodes), ΔV_1 is the net voltage change from the readout circuit, and ΔV_{out} is the output voltage. Thus, Gain1 comes from the ratio of proof mass M to net stiffness K , M/K . The Gain2 can be yielded from the relation of capacitance change ΔC and displacement ΔX ,

$$\Delta C \cong \left. \frac{\partial}{\partial g} \left(\frac{\varepsilon A}{g} \right) \right|_{g=g_0} = \frac{C_0}{g_0} \Delta x \quad (1)$$

where g_0 is the initial gap between the stationary and moving electrodes, A is the area of sensing electrode, ε is the dielectric constant, and C_0 is the net initial capacitance for one sensing electrode pair. Moreover, Gain3 can be yielded from the relation of net voltage change ΔV_1 and capacitance change ΔC ,

$$\begin{aligned} \Delta V_1 &= V_m \left(N \frac{C_0 + \Delta C}{C_p + 4NC_0} - N \frac{C_0 + \Delta C}{C_p + 4NC_0} \right) \\ &\quad - V_m \left(N \frac{C_0 + \Delta C}{C_p + 4NC_0} - N \frac{C_0 + \Delta C}{C_p + 4NC_0} \right) \\ &= \frac{4NV_m}{C_p + 4NC_0} \Delta C \end{aligned} \quad (2)$$

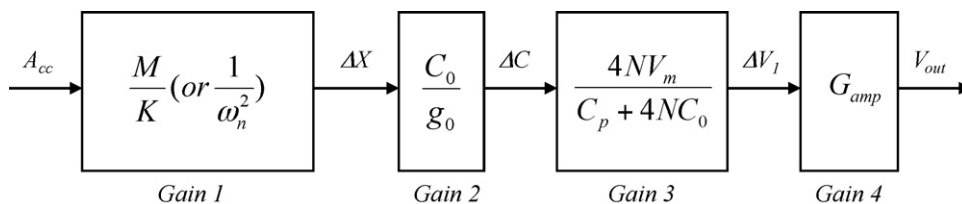


Fig. 2. The gain flow chart of the present accelerometer.

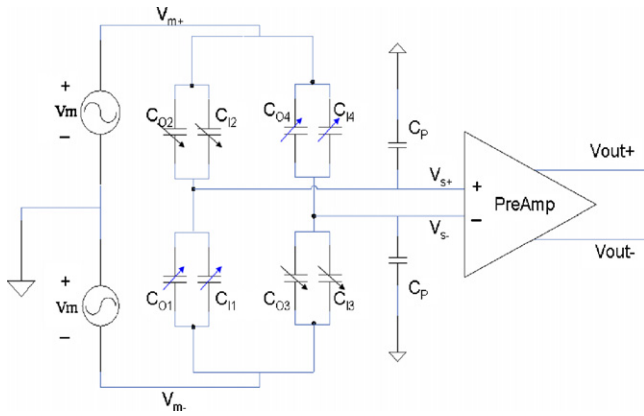


Fig. 3. Simplified sensing schematic.

where $2N$ is the total number of sensing electrode pairs, V_m is a specified modulation voltage, and C_p is the net parasitic capacitance. The pre-amplifier in this study acted as a buffer with a gain (Gain4) of 1. In summary, the net gain (Gain)_{net} of this study gives a sensitivity of the present accelerometer of,

$$(\text{Gain})_{\text{net}} = \frac{V_{\text{out}}}{A_{\text{cc}}} = \frac{M}{K} \frac{C_0}{g_0} \frac{4NV_m}{(C_p + 4NC_0)} \quad (3)$$

In general, the present design can increase the number of sensing electrodes by 1.8-fold at the cost of the decreasing of 20% proof mass. However, the rest of parameters in Eq. (3) remain the same. According to Eq. (3), the net sensitivity of the accelerometer will still be increased by 1.44-fold without changing its die size. Moreover, consider the present accelerometer which has the same die size and fundamental frequency as those of Fig. 1a. In this case, these two accelerometers have the same stiffness to mass ratio K/M (and vice versa, M/K). Thus, the increasing of net sensitivity of the accelerometer is mainly influenced by the total number of sensing electrode pairs $2N$, and can even be increased by 1.8-fold without changing its die size. The sensing electrodes are connected as a fully differential capacitive bridge with modulation signal, as shown in Fig. 3. The sensing capacitances of $C_{O(1,2,3,4)}$ and $C_{I(1,2,3,4)}$ were connected to the pre-amplifier. The C_p includes the parasitic capacitances of not only wires but also structures. The pre-amplifier circuit schematic acted as a buffer for output signal [5]. It is a standard two-stage cascode differential amplifier. The diode-connected transistor was employed to implement the DC path on the capacitive input node of the pre-amplifier.

3. Fabrication and testing

The accelerometer was realized using the TSMC 0.35 μm 2P4M CMOS process, as shown in Fig. 4a. After that, the reactive ion etching (RIE) anisotropic etching was used to remove the silicon dioxide, as shown in Fig. 4b. In this process, the top metal layer was employed to act as the etching mask. Finally, the substrate was etched isotropically using XeF_2 to suspend the mechanical components, as illustrated in Fig. 4c. Fig. 5a shows the scanning electron microscopy (SEM) photo of a typical fabrication results. The key components such as the hollow proof

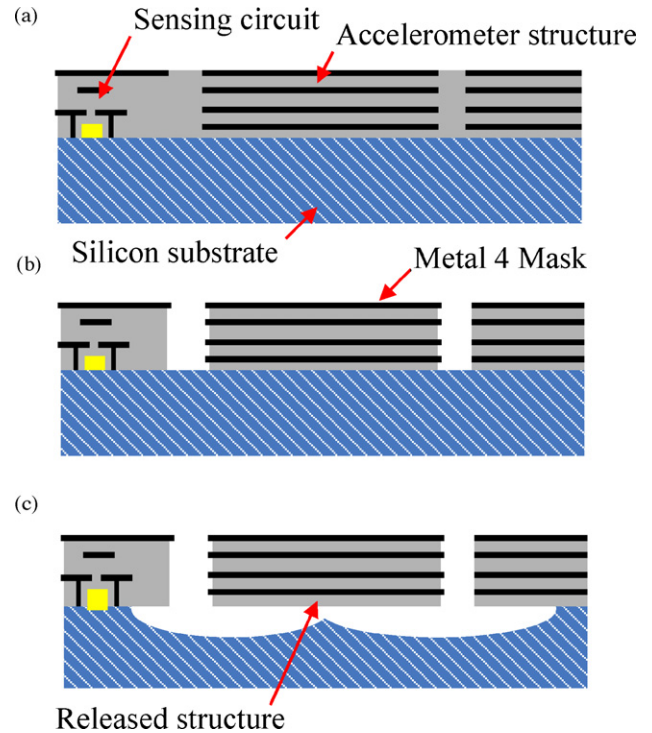


Fig. 4. Fabrication steps: (a) after TSMC 0.35 μm 2P4M CMOS process, (b) RIE remove silicon oxide, and (c) structure releasing by XeF_2 isotropic etching.

mass, center post, supporting and routing springs, sensing electrodes, self-diagnostic actuators, and curvature matching frame are clearly observed in the photo. In addition, the sensing electrodes are distributed at both the inner and outer edges of the hollow proof mass. Fig. 5b shows the zoom in SEM photo of

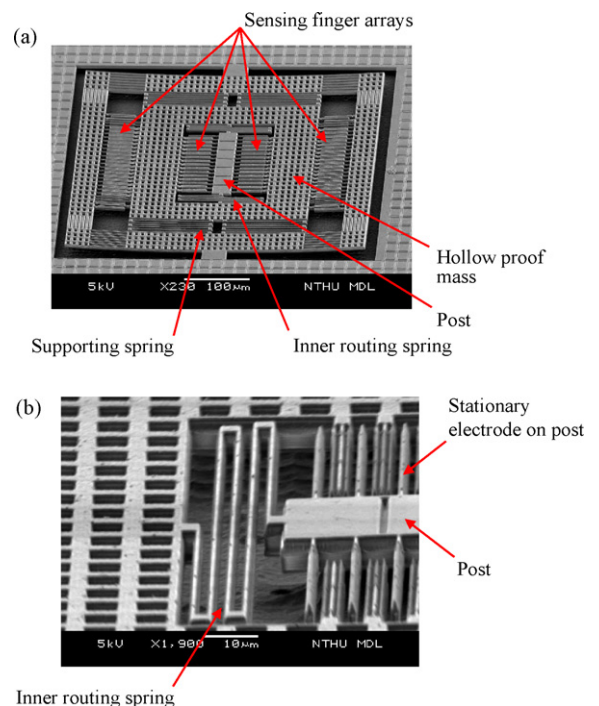


Fig. 5. (a) The SEM photo of a typical fabricated accelerometer, and (b) the zoom in photo to show the inner spring for electrical routing.

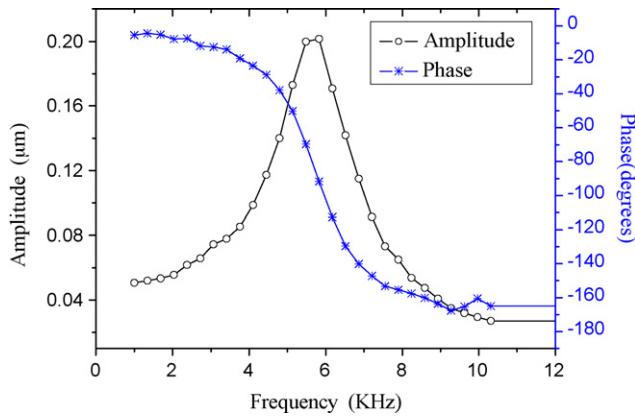


Fig. 6. The typical measured frequency responses and the associated phase diagram of the accelerometer in Fig. 5, and the natural frequency of the accelerometer was 5.83 Hz.

the inner routing spring between the post and the proof mass. The photo also demonstrates that the proof mass and spring are successfully suspended on the substrate, whereas the post still anchors to the substrate. Moreover, the stationary and movable comb sensing electrodes are also observed.

In this study, the size of accelerometer was $440\ \mu\text{m} \times 490\ \mu\text{m}$. Its proof mass and the net spring stiffness were designed to be 0.85 ng and 0.98 N/m, respectively. Thus, the system has a Gain1 of 8.48 nm/G. During the test, the accelerometer was firstly driven electrostatically by the self-diagnostic comb actuators. After driven with a harmonic excitation, the typical frequency response of the accelerometer was characterized in Fig. 6. The resonant frequency of this accelerometer was 5.83 kHz, and the Gain1 was extracted to be 7.55 nm/G. Thus, the measured and the predicted Gain1 have 11% difference. Moreover, this test also demonstrated the feasibility of the self-diagnostic actuator. As shown in Fig. 7, the test setup has been established to determine the sensitivity and linearity of accelerometer. In this test, the packaged accelerometer, as shown in the insets of Fig. 7, was driven by the shaker. The sensing signal was measured and displayed using a spectrum analyzer. Moreover, the dynamic characteristic of the shaker was monitored using a commercial accelerometer. Fig. 8 shows the typical results measured from the accelerometer after driven by shaker with a 5 V, and 100 Hz (i.e. 5 G) harmonic (sinusoidal) excitation. The noise floor is 0.1 G/ $\sqrt{\text{Hz}}$ with a modulation voltage of 1 V at 1 MHz.

The square dots in Fig. 9 show the variation of the output voltage of the accelerometer with the excitation amplitude. Thus, the sensitivity and the nonlinearity of the present accelerometer are 3.95 mV/G, and 2.75%, respectively. On the other hand, the predicted net initial capacitance of sensing electrodes was 1.65 fF/pair, and the present accelerometer had 68 sensing electrode pairs ($N=34$). Moreover, the initial gap of sensing electrodes g_0 was 1.5 μm , and the modulation voltage V_m was specified as 1 V. According to the simulation from HSPICE, the net parasitic capacitance C_p was 300 fF, hence, the net gain predicted by Eq. (3) gave a sensitivity of the present accelerometer of 4.36 mV/G. The measured and predicted sensitivity has 9.4% deviation. This is mainly resulted from the mismatch of the real

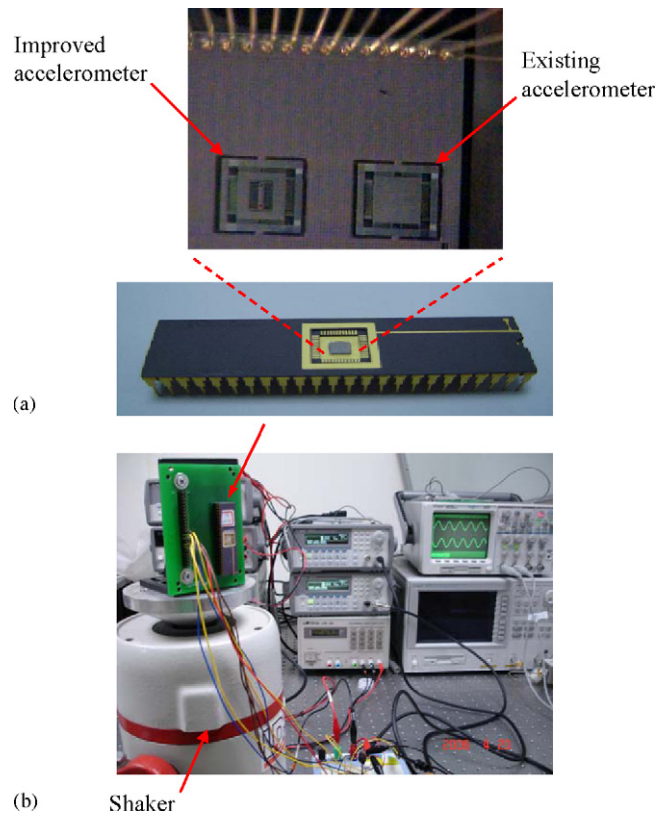


Fig. 7. (a) The photo of a packaged accelerometer, and (b) the experiment setup for shaker vibration test on the packaged accelerometer.

and assumed net parasitic capacitance C_p , and the mismatch of the geometry shape of structures due to micro fabrication.

As a comparison, this study also fabricated the accelerometer of existing design in Fig. 1a. This reference accelerometer had the same size ($440\ \mu\text{m} \times 490\ \mu\text{m}$) and fundamental frequency as those of the one in Fig. 1b. Thus, these two accelerometers had very close mass to stiffness ratio. However, the total sensing electrode pairs dropped from 68 to only 38 ($N=19$). As shown in Fig. 10, the measured fundamental frequency of this reference accelerometer (5.92 kHz) agrees well with that of the improved one (5.83 kHz). In addition, the measurement results in Fig. 9

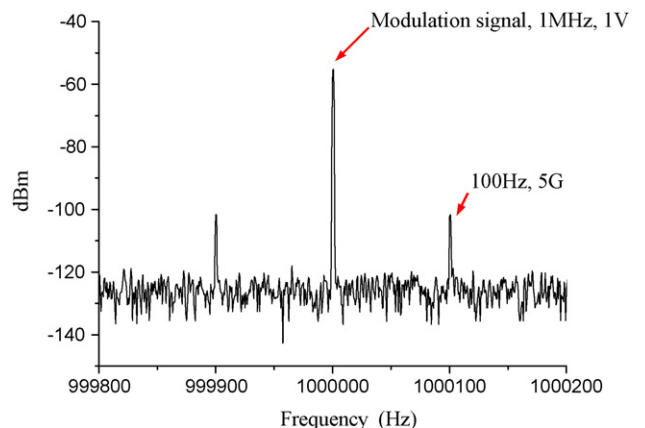


Fig. 8. Spectrum of the accelerometer output signal when driven by an excitation of 100 Hz, 5 V (5 G) using shaker.

Table 1
The characteristics of the present accelerometer, and its comparison with the existing design

	Designs	
Axes	1	1
Measurement range (G)	0.3–10 G	0.7–10 G
Sensitivity (V/G)	3.95 mV/G	2.1 mV/G
Resonant frequency (kHz)	5.83 kHz	5.92 kHz
Modulation voltage (V)	1 V, 1 MHz	1 V, 1 MHz
Nonlinearity (%FS)	±2.75%FS	±2.87%FS

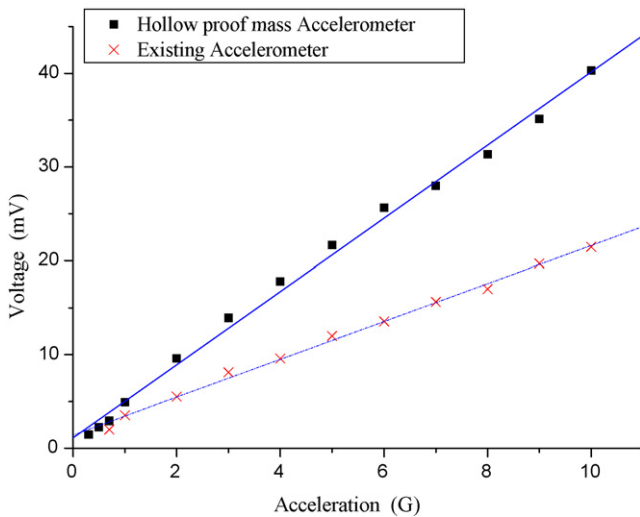
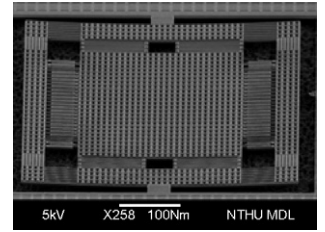
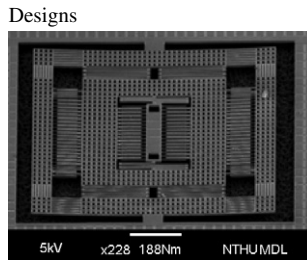


Fig. 9. Variation of the measured output voltage with the specified input acceleration, the square dots indicate the present accelerometer, and the cross dots represent the existing design.

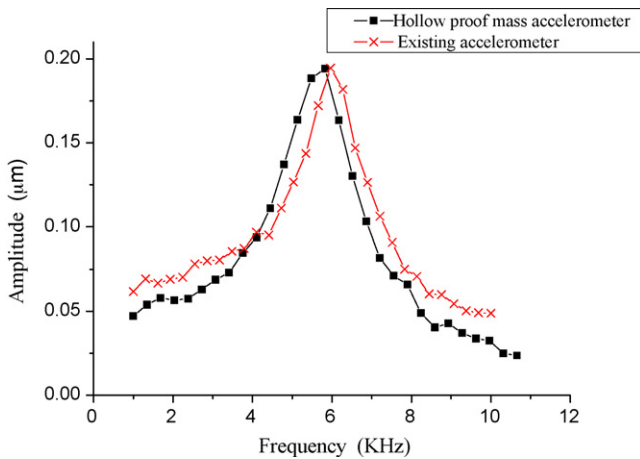


Fig. 10. Comparison of the measured frequency responses for the existing (5.92 kHz) and present (5.83 kHz) accelerometers.

show that the sensitivity of the improved design is 1.88-fold higher than the reference accelerometer (with the same fundamental frequency). The measurement agrees well with the results predicted in Section 2. The testing also shows that the minimum measurable range had been increased from 0.7 to 0.3 G. The comparison of these two accelerometers is summarized in Table 1.

4. Conclusions

This study presents an improved CMOS capacitance accelerometer with more sensing finger arrays. To implement the present concept, the additional springs and anchor-post are exploited in this CMOS accelerometer for electrical routing of sensing finger arrays. The feasibility of the CMOS accelerometer has been demonstrated using the TSMC 2P4M process. The measurement results show that the sensitivity and the nonlinearity of a typical improved accelerometer are 3.95 mV/G, and 2.75%, respectively. As a comparison, the existing accelerometer of the same die size and fundamental frequency (i.e. the same mass to stiffness ratio) has the sensitivity and the nonlinearity of 2.10 mV/G, and 2.87%, respectively. The results demonstrate that the present design has successfully improved the sensitivity of the CMOS capacitance accelerometer by 1.88-fold without changing the die size.

Acknowledgements

This research was sponsored in part by Delta Electronics Inc and the National Science Council of Taiwan under grant of NSC-94-2212-E-007-026. The authors wish to appreciate the National Chip Implementation Center (CIC), Taiwan, for supporting the IC Manufacturing. The authors would like to thank the Central Regional MEMS Research Center of National Science Council, Semiconductor Research Center of National Chiao Tung University and National Nano Device Laboratory of NSC for providing the fabrication facilities.

References

- [1] <http://www.sandia.gov>.
- [2] S.J. Sherman, Monolithic accelerometer, U.S.A. Patent No. 5345824S, Analog Devices, Inc. September 13, 1994.
- [3] L.R. Carley, M.L. Reed, G.K. Fedder, Microelectromechanical structure and process of making same, U.S.A. Patent No. 5,717,631. Carnegie Mellon University, February 10, 1998.
- [4] H. Luo, G. Zhang, L.R. Carley, G.K. Fedder, A post-CMOS micromachined lateral accelerometer, *IEEE/ASME J. MEMS* 11 (2002) 188–195.
- [5] J.M. Tsai, G.K. Fedder, Mechanical noise-limited CMOS-MEMS accelerometers, in: MEMS'05, Miami Beach, FL, January 30–February 3, 2005, pp. 630–633.
- [6] H. Xie, G.K. Fedder, Z. Pan, W. Frey, Design and fabrication of an integrated CMOS-MEMS 3-axis accelerometer, in: MSMS'03, San Francisco, CA, February 23–27, 2003, pp. 292–295.
- [7] H. Lakdawala, G.K. Fedder, Temperature stabilization of CMOS capacitive accelerometer, *IEEE/ASME J. MEMS* 13 (2004) 559–566.
- [8] K. Klaus, K. Norbert, K. Holger, M. Wilfried, Capacitive pressure sensor with monolithically integrated CMOS readout circuit for high temperature applications, *Sens. Actuators A* 97/98 (2002) 83–87.
- [9] E. Socher, O. Degani, Y. Nemirowsky, Optimal design and noise considerations of CMOS compatible IR thermoelectric sensors, *Sens. Actuators A* 71 (1998) 107–115.
- [10] H. Luo, X. Zhu, H. Lakdawala, R. Carley, G. Fedder, A copper CMOS-MEMS Z-axis gyroscope, in: MEMS'02, Las Vegas, NV, January 20–24, 2002, pp. 631–634.
- [11] H. Xie, G. Fedder, Fabrication, characterization, and analysis of a DRIE CMOS-MEMS gyroscope, *IEEE Sens. J.* (2003) 622–631.
- [12] M. Graf, R. Jurischka, D. Barrettino, A. Hierlemann, 3D nonlinear modeling of microhotplates in CMOS technology for use as metal-oxide-based gas sensors, *J. Micromech. Microeng.* 15 (2005) 190–200.
- [13] H. Seidel, U. Fritsch, R. Gottinger, J. Schalk, J. Walter, K. Ambaum, A piezoresistive silicon accelerometer with monolithically integrated CMOS-circuitry, in: Transducers'95, Stockholm, Sweden, June 25–29, 1995, pp. 597–600.
- [14] U.A. Dauderstadt, P.M. Sarro, S. Middelhoek, Temperature dependence and drift of a thermal accelerometer, in: Transducers'97, Chicago, IL, June, 1997, pp. 1209–1212.
- [15] O. Degani, D. Seter, E. Socher, S. Kaldor, Y. Nemirowsky, Micromachined accelerometer with modulated integrative differential optical sensing, *Electron. Lett.* 34 (1998) 654–655.

Biographies

Chih-ming Sun was born in Taipei, Taiwan, in 1981. He received his master degree from the Institute of NanoEngineering and MicroSystems, National Tsing Hua University in 2006. Currently he is studying for PhD degree in NanoEngineering and MicroSystems Institute, National Tsing Hua University, Taiwan. His major research interests include CMOS MEMS capacitive sensors, CMOS MEMS post processing, and system integration.

ChuanWei Wang was born in Taoyuan, Taiwan, in 1978. He received his master degree from the Mechanical and Macaronic Engineering Department of National Taiwan Ocean University in 2003. Currently he is studying for the PhD degree in Power Mechanical Engineering Department, National Tsing Hua University, Taiwan. His major research interests include capacitive inertial sensors, capacitive interface circuits, and system control.

Weileun Fang was born in Taipei, Taiwan, in 1962. He received his PhD degree from Carnegie Mellon University in 1995. His doctoral research focused on the determining of the mechanical properties of thin films using micromachined structures. In 1995, he worked as a postdoctoral research at Synchrotron Radiation Research Center, Taiwan. He joined the Power Mechanical Engineering Department at the National Tsing Hua University (Taiwan) in 1996, where he is now a professor as well as a faculty of MEMS Institute. From June to September 1999, he was with Prof. Y.-C. Tai at California Inst. Tech. as a visiting associate. He has established a MEMS testing and characterization lab. His research interests include MEMS with emphasis on micro fabrication/packaging technologies, micro optical systems, microactuators, and the characterization of the mechanical properties of thin films.